Intensity dependence narrowing of electromagnetically induced absorption in a Doppler-broadened medium

J. Dimitrijević,[*] D. Arsenović, and B. M. Jelenković

Institute of Physics, 11080 Belgrade, Serbia
(Received 13 April 2007; published 27 July 2007)

In this paper, we present a theoretical model for studying the interaction between linearly polarized laser light and near-degenerated Zeeman sublevels for a multiple V-type atomic system of $^2S_{1/2}F_g=2 \rightarrow {}^2P_{3/2}F_e=3$ transition in ^{87}Rb. We have calculated the laser absorption in a Hanle configuration, as well as the amplitudes and the widths of electromagnetically induced absorption (EIA) in the range of laser intensities from 0.01 to 40 mW/cm^2. Our results, showing nonvanishing EIA amplitude, a nonmonotonic increase of the EIA width for the increase of laser intensity, and pronounced shape differences of the Hanle EIA curves at different laser intensities, are in good agreement with recent experimental results. We have found that the EIA behaves differently than the electromagnetically induced transparency (EIT) as a function of the laser intensity. Both the amplitude and width of the EIA have narrow maximums at 1 to 2 mW/cm^2. We have shown the strong influence of Doppler broadening of atomic transition on Hanle resonances and have suggested the explanation of it.

PACS number(s): 42.50.Gy, 32.70.Jz

I. INTRODUCTION

Electromagnetically induced transparency (EIT) [1] and absorption (EIA) [2] are two opposite effects of optical pumping and coherence: in the EIT, the medium is characterized by sub-Doppler transmission and normal dispersion, while in the EIA it is characterized by narrow absorption gain and abnormal dispersion. Both EIT and EIA can be induced between either hyperfine levels or Zeeman sublevels, but atomic schemes required for them are different. Λ-atomic schemes, and $F_g \geq F_e$, are necessary for the EIT, while V-atomic schemes, and $0 < F_g < F_e$, are required for EIA [3,4]. Depending on the choice of quantization axes, both EIT and EIA can be explained either by optical pumping or by coherence [5–8]. While coherences in the EIT are formed between lower (long-lived) levels, coherences in the EIA are induced between upper levels of the V-scheme, subsequently transferred via spontaneous emission to lower hyperfine levels [8]. Both EIA and EIT were studied by using two-photon resonance in either of two configurations—bichromatic probe-pump or Hanle, where the laser transmission and the fluorescence were measured and calculated. In the latter, a single laser excites a two-level atom while the external magnetic field varies around zero.

The EIT has been known long before and investigated much more than the EIA. The interest for the EIT exists because of interesting applications in magnetometers [9] and miniature atomic clocks [10]. Lately, there is new interest in both the EIT and EIA because the steepness of the dispersion at the resonance [11,12] allows both fascinating changes and the control of the group velocities of light propagating through the medium with both normal (EIT) and abnormal (EIA) dispersion [13–18]. The control of light pulses by means of resonant laser-atom interaction creates a fundamentally new area of laser applications in information process-

ing, communications, spectroscopy, and material science. Studying the dependence of resonance shapes, widths, and amplitudes on experimental parameters is of great interest.

In this work, we present the theoretical results of the EIA behavior as a function of the laser intensity. The effects arising from the influence of laser intensity on EIT widths were investigated in several papers. Javan *et al.* [19] gave an analytical expression for the widths as a function of the laser intensity. The dependence of the EIT resonance width on the laser pump intensity, observed in an Λ-system between hyperfine levels, was recently studied experimentally [20]. More references on the experiments with the EIT width can be found in [20]. There are only a few papers dealing with the effects of laser intensity influence on the EIA, in either pump-probe or Hanle configuration. Akulshin *et al.* [2], in a two-level weakly degenerated atomic system, showed dependence of the probe transmission resonance on the pump laser intensity for closed transitions in the D2 line in both 85 and 87 Rb isotopes. They showed linear dependence of the probe linewidth at lower pump laser intensities (below 1 mW/cm^2), and slower intensity dependence as laser intensity increases. Lipsich *et al.* [21] showed the absorption properties of the probe laser in a degenerated two-level system, driven by the pump laser, with different pump laser Rabi frequencies, for different atomic systems, including the case $F_g=F_e-1$ for which the EIA can be observed. Mollela *et al.* [22] have measured the widths of the pump laser for the Cs D2 line of closed hyperfine transition, and have shown a nearly linear increase from ~10 to 50 kHz as a function of two-photon detuning, for the power range of the probe laser between 20 μW and 2 mW. The theoretical work of the Hanle EIA dependence on the laser intensity was done by Renzoni *et al.* [23]. For linearly polarized light, for closed $F_g=3 \rightarrow F_e=4$ in ^{85}Rb and $F_g=2 \rightarrow F_e=3$ in ^{87}Rb transitions, they observed, by analytically and numerically solving the optical Bloch equations, that EIA vanished at laser intensities around a few mW/cm^2. They did not include the Doppler broadening of atomic transitions.

————
*[*]jelenad@phy.bg.ac.yu
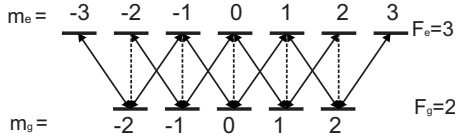
FIG. 1. Level diagram for the $F_g=2 \rightarrow F_e=3$ transition of ^{87}Rb. Full lines stand for transitions induced by linearly polarized laser light, while both full and dashed lines describe spontaneous emission.

Experimentally, both EIT and EIA were studied in Doppler-broadened media, in vacuum cells, or in cells with buffer gases. Doppler broadening is an important effect in lasers interactions with gaseous media, and many important phenomena, like hole burning [24] and Lamb dip [25] are related to it. Doppler broadening also affects EIT and EIA line profiles. It was found [19] that the EIT width in the Doppler-broadened medium is smaller than in the medium with homogenous broadening, due to the reduced power broadening for the off-resonant atoms. As for the effects of the Doppler broadening on the EIA, narrowing, i.e., reducing of the EIA width by increasing the Doppler width, was indicated by Brazhnikov *et al.* [26] for Hanle configuration. Taking into account the Doppler effect, it was possible to successfully model the experimental results of the dependence of the Hanle EIA amplitude and width on the laser light polarization [27].

Recent experimental results [28] have shown that the width and the amplitude of the Hanle EIA have different dependences on the laser intensity, compared to the width and the amplitude of the EIT. The theoretical model presented in [28] did not take into account the Doppler broadening and was not able to simulate experimental results very well. We have had strong motivation to improve the model and to explain such specific behavior of the EIA. In the present paper, we give the theoretical explanation of results in Ref. [28]. We have calculated the density matrix elements for the full system of optical Bloch equations for the transition $F_g=2 \rightarrow F_e=3$ in ^{87}Rb, and then have averaged the results assuming the Maxwell-Boltzmann velocity distribution at room temperature. Our results show the strong effect of Doppler broadening on the shapes, amplitudes, and widths of the Hanle EIA, as well as on the atomic population on different laser intensities. We are not aware of previous theoretical results studying the behavior of the Hanle EIA width and amplitude as a function of laser intensity in a Doppler-broadened media.

II. THEORETICAL MODEL

In this section we present the model used to calculate the EIA, i.e., the absorption of a laser beam, resonant to the closed $F_g=2 \rightarrow F_e=3$ transition of ^{87}Rb (see Fig. 1) as a function of applied magnetic field B_{scan}. Zeeman sublevels are coupled by the linearly polarized laser field propagating along the z axis, which is the direction of the B_{scan}. The incident laser beam is linearly polarized along the x axis:

$$\vec{E}(\vec{r}_0,t) = \vec{e}_x \cos(\omega_{(1)}t)E_{(1)0x} = \frac{\vec{u}_{-1} - \vec{u}_{+1}}{2\sqrt{2}} e^{-i\omega_{(1)}t}E_{(1)0x}. \quad (1)$$

Here $\omega_{(1)}$ is the laser frequency, $E_{(1)0x}$ is the amplitude of the laser electric field, and $\vec{u}_{\pm 1}$ are unit vectors of a rotation coordinate system ($\vec{u}_{-1} = \frac{\vec{e}_x - i\vec{e}_y}{\sqrt{2}}$, $\vec{u}_{+1} = -\frac{\vec{e}_x + i\vec{e}_y}{\sqrt{2}}$). We have solved optical Bloch equations for density matrix elements $\rho_{i,j}$ for the system of all magnetic sublevels of the ground $F_g=2$ and the excited $F_e=3$ states. Studying the full (real) system reveals optical pumping and multiple coherences, which do not exist in a simpler atomic scheme. The optical Bloch equations for the closed system, and including the ground state relaxation, have the form

$$\dot{\varrho}_{e_i e_j} = \left(-\frac{2}{7}\Gamma_L|\mathcal{G}_1|^2 + i(\omega_{e_j} - \omega_{e_i}) \right)\varrho_{e_i e_j}$$

$$+ i\mathcal{G}_{2x}\sum_{l=-2}^{2} [\tilde{\varrho}_{e_i g_l}(-\mu_{g_l,e_j,-1} + \mu_{g_l,e_j,1})$$

$$+ (\mu_{e_i,g_l,-1} - \mu_{e_i,g_l,1})\tilde{\varrho}_{g_l e_j}] - \gamma\varrho_{e_i e_j},$$

$$\dot{\tilde{\varrho}}_{e_i g_j} = \left(-\frac{\Gamma_L}{7}|\mathcal{G}_1|^2 + i(\omega_{(1)} + \omega_{g_j} - \omega_{e_i}) \right)\tilde{\varrho}_{e_i g_j}$$

$$+ i\mathcal{G}_{2x}\left(\sum_{l=-3}^{3} [\varrho_{e_i e_l}(-\mu_{e_l,g_j,-1} + \mu_{e_l,g_j,1})] \right.$$

$$\left. + \sum_{l=-2}^{2} [(\mu_{e_i,g_l,-1} - \mu_{e_i,g_l,1})\varrho_{g_l g_j}] \right) - \gamma\tilde{\varrho}_{e_i g_j},$$

$$\dot{\tilde{\varrho}}_{g_j e_i} = \left(-\frac{\Gamma_L}{7}|\mathcal{G}_1|^2 + i(-\omega_{(1)} + \omega_{e_i} - \omega_{g_j}) \right)\tilde{\varrho}_{g_j e_i}$$

$$+ i\mathcal{G}_{2x}\left(\sum_{l=-2}^{2} [\varrho_{g_j g_l}(-\mu_{g_l,e_i,-1} + \mu_{g_l,e_i,1})] \right.$$

$$\left. + \sum_{l=-3}^{3} [(\mu_{g_j,e_l,-1} - \mu_{g_j,e_l,1})\varrho_{e_l e_i}] \right) - \gamma\tilde{\varrho}_{g_j e_i},$$

$$\dot{\varrho}_{g_i g_j} = \left(2\sum_{q=-1}^{1} \mu_{e_{i+q},g_i,q}\mu^*_{e_{j+q},g_j,q}\varrho_{e_{i+q}e_{j+q}}\Gamma_L + i(\omega_{g_j} - \omega_{g_i})\varrho_{g_i g_j} \right)$$

$$+ i\mathcal{G}_{2x}\sum_{l=-3}^{3} [\tilde{\varrho}_{g_i e_l}(-\mu_{e_l,g_j,-1} + \mu_{e_l,g_j,1})$$

$$+ (\mu_{g_i,e_l,-1} - \mu_{g_i,e_l,1})\tilde{\varrho}_{e_l g_j}] - \gamma\left(\varrho_{g_i g_j} - \frac{1}{5}\delta_{ij} \right), \quad (2)$$

where g and e refer to the ground and the excited state hyperfine levels, respectively. Fast oscillations at laser frequency $\omega_{(1)}$ in Eq. (2) were eliminated by the usual substitution

$$\varrho_{e_i g_j} = \tilde{\varrho}_{e_i g_j}e^{-i\omega_{(1)}t}. \quad (3)$$

In Eq. (2), $\mu_{a,b,q} = e\langle a|\vec{u}_q\vec{r}|b\rangle$, where the symbols a and b indicate any ground or excited Zeeman sublevel given by the
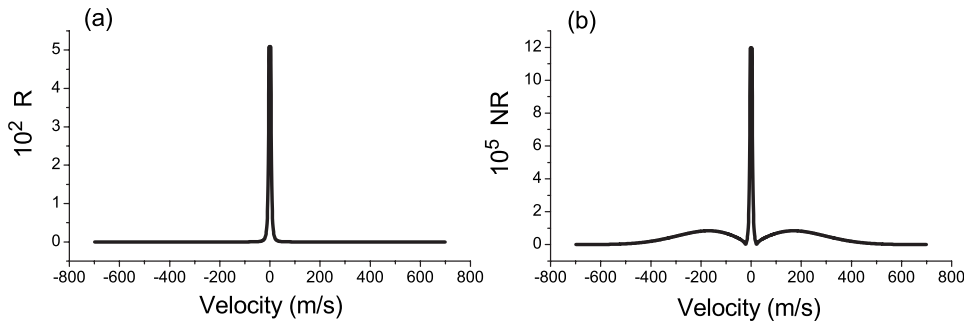
FIG. 2. Calculated functions (a) $R(v)$ and (b) $NR(v)$.

quantum number $m_{g(e)}$. $\mathcal{G}_1$ is the constant proportional to the reduced matrix element of the dipole operator between the ground and the excited states

$$\mathcal{G}_1 \sim \langle n_e L_e \| \vec{r} \| n_g L_g \rangle. \qquad (4)$$

The value of the reduced matrix element is taken from [29]. The expression for μ then becomes

$$\mu_{m_e, m_g, q} = \mathcal{G}_1 (-1)^{m_e} \begin{pmatrix} 2 & 1 & 3 \\ m_g & q & -m_e \end{pmatrix}, \qquad (5)$$

where $q = 0, \pm 1$. The amplitude of the laser electric field enters Eq. (2) via

$$\mathcal{G}_{2x} = \frac{E_{(1)0x}}{2\sqrt{2}\hbar}. \qquad (6)$$

The light Rabi frequency of the individual transition is

$$\Omega_{R_{m_e, m_g, q}} = \mathcal{G}_{2x} \mu_{m_e, m_g, q}$$

$$= \frac{E_{(1)0x}}{2\sqrt{2}\hbar} \mathcal{G}_1 (-1)^{-m_e} \begin{pmatrix} 2 & 1 & 3 \\ m_g & q & -m_e \end{pmatrix}$$

$$= \frac{1}{2\sqrt{2}\hbar} \sqrt{\frac{2I}{c\varepsilon_0}} \mathcal{G}_1 (-1)^{-m_e} \begin{pmatrix} 2 & 1 & 3 \\ m_g & q & -m_e \end{pmatrix}, \quad (7)$$

where I is the laser intensity. Through this equation we were able to present the theoretical results at specific laser intensity and to directly compare them with the results from the experiment [28].

In Eq. (2), energies describing the Zeeman splitting of the ground and the excited levels with quantum numbers $m_{g(e)}$, $E_{g(e)} = \omega_{g(e)}\hbar$, due to applied magnetic field B_{scan}, were calculated using

$$E_{g(e)} = \mu_B g_{F_{g(e)}} m_{g(e)} B_{scan}. \qquad (8)$$

Here μ_B is the Bohr magneton and $g_{F_{g(e)}}$ is the Lande gyromagnetic factor for two hyperfine levels (1/2 for the ground and 2/3 for the excited state). Laser detuning, which is the
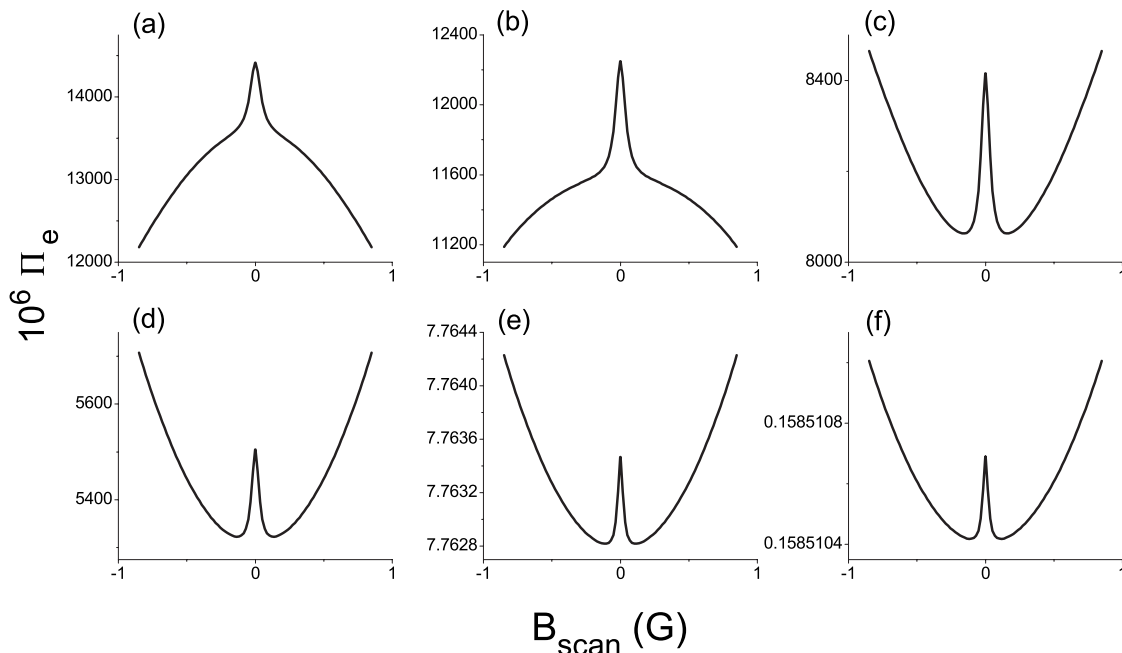
FIG. 3. Hanle EIA for the laser intensity of $I = 0.1$ mW/cm^2 for atomic velocities of (a) 0, (b) 1, (c) 2, (d) 3, (e) 100, and (f) 700 m/s.
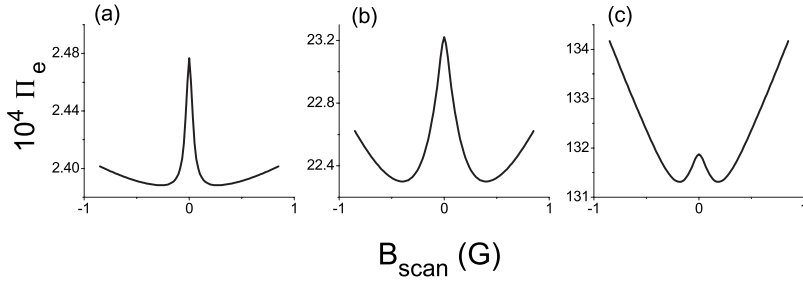
FIG. 4. Calculated Hanle EIA for (a) $I=0.1$ mW/cm^2, (b) $I=1$ mW/cm^2, and (c) $I=10$ mW/cm^2. Laser light is resonant to the $F_g=2 \rightarrow F_e=3$ transition in ^{87}Rb.

difference between laser frequency and the frequency of the D2 line is given by $\Delta_D = \omega_{(1)} - (\omega_{e_0} - \omega_{g_0})$.

In Eq. (2) $\frac{2}{7}\Gamma_L|\mathcal{G}_1|^2 = \Gamma$, where $\Gamma = 2\pi \times 6.07$ MHz is the total spontaneous emission rate of any excited sublevel. The ground state relaxation rate is given by γ. In the absence of relaxation mechanisms in the vacuum Rb cell at room temperature Rb vapor (the atom's mean free path is much longer then the cell dimensions), γ is determined by the atom transit time through the laser beam. It describes the rate at which atoms enter and leave the laser beam. Under these assumptions, we have calculated γ from $\gamma = v_{mp}/r$ [30], where $v_{mp} = \sqrt{2k_BT/M}$ is the most probable velocity of the atoms (equal to ~ 240 m/s for Rb atoms at room temperature) and r is the radius of the laser beam. We take the value for $r=1.25$ mm, which is the radius of the laser beam in [28].

The system of equations given in Eq. (2) was solved assuming a steady state of the atomic system. The steady-state solution can be compared to the experimental results of [28] because the estimated atom transit time through the laser beam is longer than the calculated time which atoms require to reach a steady-state when suddenly illuminated by light tuned to a closed transition [31]. Since all atoms in the excited state decay at the same rate, the light absorption coefficient in optically thin media is proportional to the total excited state population [32]

$$\Pi_e = \sum \varrho_{e_i e_i}. \tag{9}$$

The dependence of this quantity on B_{scan} around zero is the Hanle absorption curve and we denote it by A.

The Doppler effect was taken into account in calculations of the total light absorption by averaging absorption curves, calculated for a single atomic velocity, over velocities in the range -700 to 700 m/s according to

$$A = \sum A(v_i)w(v_i), \tag{10}$$

where $w(v_i)$ are the weights of the Maxwell-Boltzmann distribution $f(v)$. We calculated them as

$$w(v_i) = \int_{(v_{i-1}+v_i)/2}^{(v_i+v_{i+1})/2} f(v)dv. \tag{11}$$

$A(v_i)$ is the absorption curve for the range of the scanning field B_{scan} from -0.85 to 0.85 G, for a particular atomic velocity v_i, i.e., for the laser frequency detuning Δ_D (1.28 MHz per atomic velocity of 1 m/s).

How does one partition the Maxwell-Boltzmann distribution in order to considerably reduce the computation time and the errors of numerical integration? One can get an an-

swer to this question from the behavior of the curves $A(v_i)$ for atomic velocities throughout MB distribution [for $v_i \in (-700, 700)$ m/s], and more so with a help of the following functions:

$$R(v_i) = \max_{B_{scan}} |A(v_{i+1}) - A(v_i)|, \tag{12}$$

$$NR(v_i) = \max_{B_{scan}} |A(v_{i+1})f(v_{i+1}) - A(v_i)f(v_i)|. \tag{13}$$

In Figs. 2(a) and 2(b), we show the dependence of $R(v)$ and $NR(v)$ on the atomic velocity assuming uniform partition of the Maxwell-Boltzmann distribution function by 1 m/s. In approximating Doppler averaging $\int A(v)w(v)dv$ with Eq. (10), the error is less than $\Sigma_{v_i} NR(v_i)\Delta v_i$. Greater values of $NR(v_i)$ require denser partition Δv_i in order to keep the error at low levels. It follows from these results that partition of the Maxwell-Boltzman distribution need not be uniform. Instead, partition should be most dense around zero velocity. We can demonstrate the same findings by showing how the shape of the resonance (for a single atom velocity) changes as atomic velocity increases. In Figs. 3(a)–3(d) we show that the EIA shape changes rapidly for small changes in atomic velocity, when these velocities are small. Figures 3(e) and
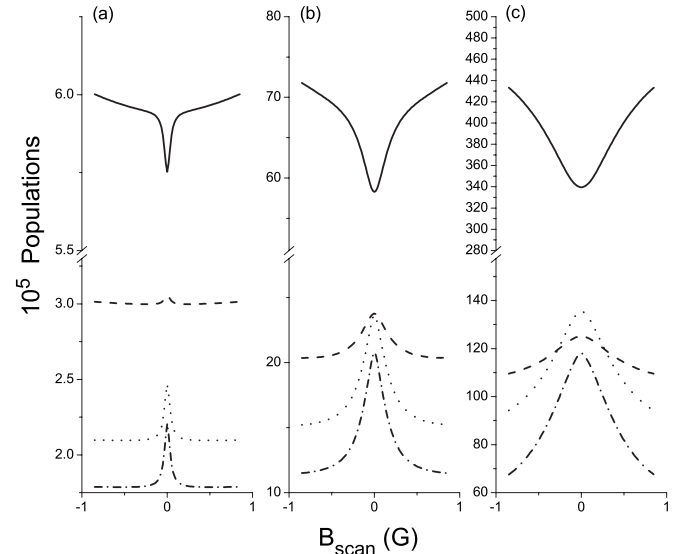
FIG. 5. Populations of excited state's sublevels as a function of the external magnetic field, for three laser intensities: (a) $I=0.1$ mW/cm^2, (b) $I=1$ mW/cm^2, and (c) $I=10$ mW/cm^2; solid curves: $|m_e|=3$, dashed curves: $|m_e|=2$, dotted curves: $|m_e|=1$, and dash-dot curves: $m_e=0$.
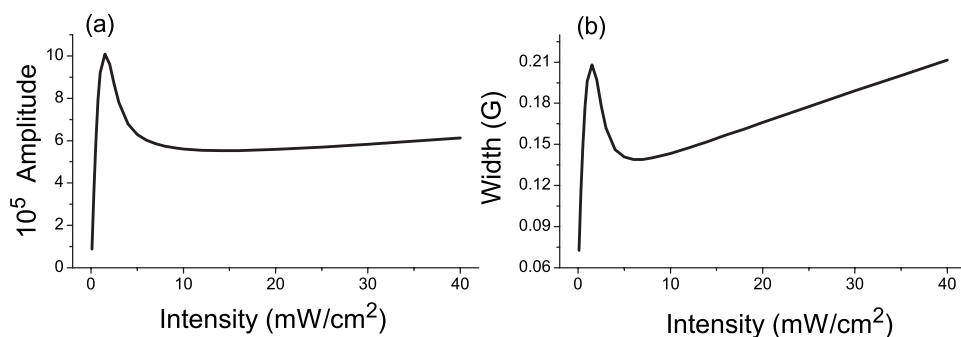
FIG. 6. Calculated EIA (a) amplitudes and (b) widths as a function of the laser intensity. Amplitudes and widths were determined from resonances of Π_e vs B_{scan}.

3(f) show, on the other hand, for large atomic velocities, how little the EIA has changed in a very large range of velocities.

III. RESULTS

Figure 4 presents the calculated EIA for the laser resonant to the $F_g=2 \rightarrow F_e=3$ transition in ^{87}Rb, as a function of the axial magnetic field at three laser intensities. The averaging over Doppler detunings was done using Eqs. (10) and (11). The spectra in Fig. 4 are similar to the experimental Hanle EIA and to the EIA in probe-pump configuration [22,28]. There is a difference, mainly in the adjacent region around the EIA, between the EIA shapes given by this model and the analytical model, which takes the Doppler effect into account, but is solved for the simpler $F_g=1 \rightarrow F_e=2$ transition [26]. The EIA resonances from Fig. 4 are also different from Hanle EIA shapes, calculated for zero velocity atoms or for atoms that move at well-defined velocity [please compare with the results in Fig. 3 calculated for the same laser intensity as for the data in Fig. 4(a), but without the Doppler averaging]. The Doppler integration alters the EIA amplitude and the shape of the adjacent spectral region. Moreover, it reproduces experimental results more accurately.

In Figs. 5(a)–5(c), we show the density matrix elements $\varrho_{e_i e_i}$ (which correspond to populations of different excited state's sublevels) as a function of the applied magnetic field B_{scan}. The results are given for the same laser intensities as for the total light absorption [Figs. 4(a)–4(c)]. The results show different behavior of edge sublevels, $|m_e|=3$ (solid curves), compared to inner sublevels ($|m_e|=2$: dashed curves, $|m_e|=1$: dotted curves, and $m_e=0$: dash-dot curves). Also, they show that relative contributions of the edge and inner Zeeman sublevels to the total absorption (Fig. 4) varies with the laser intensity. The effect of optical pumping to the edge sublevels is more pronounced at higher laser intensities [Fig.

4(c)] and therefore the overall shape of the Hanle curves [Fig. 3(c)] is more affected by the populations of edge sublevels.

The results for the EIA amplitudes and widths are given in Fig. 6. The EIA amplitude is the height of the resonance i.e., difference between Π_e at $B_{scan}=0$ and the minimum of Π_e. The width of the EIA is full width at half of the amplitude. They were calculated from Hanle curves, like the curves given in Figs. 4. The remarkable result of the data in Fig. 6(b) is the resonance narrowing, i.e., that the EIA width, for a narrow range of laser intensities, can decrease with the laser intensity. This is different from how the EIT widths change with the laser intensity. For lower pump intensity, the square-root dependence on the pump intensity was found for the EIT in [19,20], and explained by the optical pumping and the Doppler broadening [20]. The experimental Hanle EIT width, also presented in [20], show lower values of EIT width and a slower increase of the widths with the laser intensity, then for the probe-pump configuration.

Observed and calculated behavior of Hanle EIA amplitudes and widths is due to the contributions to the EIA from atoms within the large range of velocities. In order to clarify that these contributions are due to the Doppler effect, i.e., different laser detunings, we presented in Fig. 7 how the EIA amplitudes and widths behave for different but single atom velocity as laser intensity increases.

The curves given in Fig. 7 show that intensities, at which amplitudes and widths have maximums, shift towards higher values as the atomic velocity increases. They also show that the EIA for small atomic velocities vanishes as the laser intensity increases. At smaller intensities there are contributions from atoms at all velocities, while at higher intensities only atoms with high atomic velocities contribute to the EIA. The second reason for the observed maximum at 1 to 2 mW/cm^2 is that small velocities of several m/s are
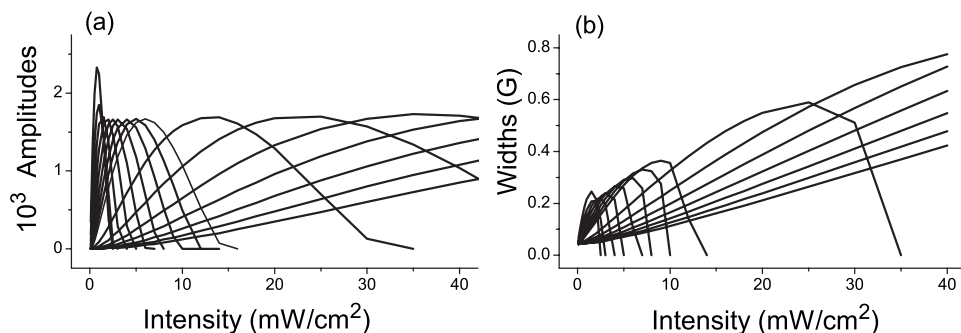
FIG. 7. Variations of EIA (a) amplitudes and (b) widths with laser intensity for different atom velocities $v_i=2-10$ (in steps of 1 m/s) and 15–45 (in steps of 5 m/s). Smaller velocities correspond to the curves with maximums at smaller intensities and vice versa.
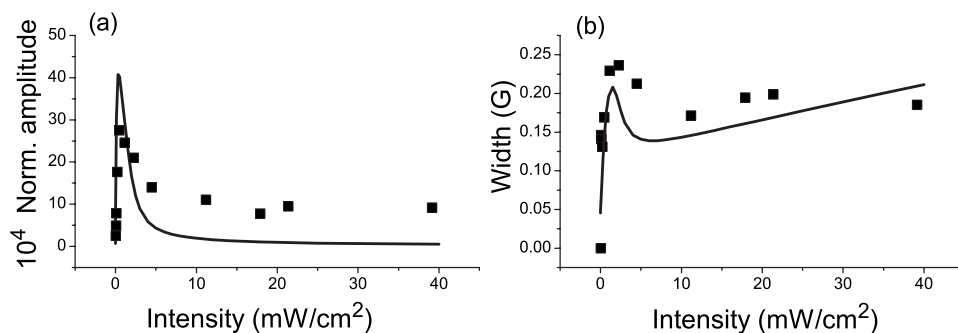
FIG. 8. Comparison with experiment of calculated and measured [28] EIA amplitudes (a) and widths (b). Amplitudes were obtained from resonances of Π_e/I, which is proportional to the absorption coefficient.

most weighed by the Maxwell-Boltzmann distribution. It is apparent from curves in Fig. 7 that the experiment with cold atoms or with an atomic beam will show that the EIA vanishes at higher laser intensity, and that laser detuning from the resonance will shift maximums of amplitude and width towards the high laser intensity.

Next, we compare the theoretical results of the amplitudes and widths of the EIA with experiment [28]. We presented these comparisons in Fig. 8. To compare the amplitudes we had to normalize the calculated amplitudes with input power (intensity). This number is still not the exact absorption coefficient because it depends on many other experimental parameters (concentration of Rb gas, temperature, diameter, and cell's length). Our theoretical results were scaled with a constant number in order to present them together with the experimental results. Our theoretical model gives widths directly in units of B_{scan} and therefore no normalization is needed to compare these results to the measurements. Calculated and measured EIA widths agree very well with the experimental data [28], while calculated EIA amplitudes show a similar narrow maximum at 1 to 2 mW/cm^2 as shown in the experiment. Therefore our model simulates the experimental observation of narrowing of the EIA as a function of the laser intensity.

IV. CONCLUSION

We have presented a theoretical framework for the analyses of EIA induced through interaction of the laser with two near-degenerate atomic systems with multiple Zeeman sublevels in the external magnetic field. The model calculates the laser absorption in the Hanle configuration for the transition $F_g=2 \rightarrow F_e=3$ in ^{87}Rb. The model takes into account the Doppler effect by averaging the Hanle absorption curves over atomic velocities within the Maxwell-Boltzmann distribution for Rb atoms at room temperature. Changes in the EIA Hanle curve throughout the Maxwell-Boltzmann distribution are most drastic for small velocities, whereas for higher velocities they are negligible. Therefore we partitioned the Maxwell-Boltzmann distribution at velocity bins whose widths are increasing with atomic velocities. Our results for the resonance line shapes, and the EIA amplitudes and widths, show qualitative and quantitative agreement with the experiment. We have theoretically confirmed that the EIA width behaves differently then the EIT with the laser intensity. We explained observed maximum of the EIA width at 1 to 2 mW/cm^2 by the facts that (a) the EIA varies differently with the laser intensity depending on the atomic velocity and (b) small atomic velocities are most weighted by the Maxwell-Boltzmann distribution. Without the Doppler effect included in theoretical model, we could not explain all of the above. Therefore we believe the Doppler effect makes a great contribution to the observed behavior of the EIA.

[1] E. Arimondo, Prog. Opt. **35**, 257 (1996).

[2] A. M. Akulshin, S. Barreiro, and A. Lezama, Phys. Rev. A **57**, 2996 (1998).

[3] Y. Dancheva, G. Alzetta, S. Cartaleva, M. Taskov, and Ch. Andeeva, Opt. Commun. **178**, 103 (2000).

[4] G. Alzetta, S. Cartaleva, Y. Dancheva, Ch. Andreeva, S. Gozzini, L. Botti, and A. Rossi, J. Opt. B: Quantum Semiclassical Opt. **3**, 181 (2001).

[5] S. I. Kanorsky, A. Weis, J. Wurster, and T. W. Hansch, Phys. Rev. A **47**, 1220 (1993).

[6] C. Goren, A. D. Wilson-Gordon, M. Rosenbluh, and H. Friedmann, Phys. Rev. A **67**, 033807 (2003).

[7] H. Failache, P. Valente, G. Ban, V. Lorent, and A. Lezama, Phys. Rev. A **67**, 043810 (2003).

[8] A. V. Taichenachev, A. M. Tumaikin, and V. I. Yudin, Phys. Rev. A **61**, 011802(R), (1999).

[9] Marlan O. Scully and Michael Fleischhauer, Phys. Rev. Lett. **69**, 1360 (1992).

[10] J. Kitching, S. Knappe, L. Liew, J. Moreland, P. D. D. Schwindt, V. Shah, V. Gerginov, and L. Hollberg, Metrologia **42**, S100 (2005).

[11] D. Budker, D. F. Kimball, S. M. Rochester, V. V. Yashchuk, and M. Zolotorev, Phys. Rev. A **62**, 043403 (2000).

[12] A. M. Akulshin, S. Barreiro, and A. Lezama, Phys. Rev. Lett. **83**, 4277 (1999).

[13] Michael M. Kash, Vladimir A. Sautenkov, Alexander S. Zi-

brov, L. Hollberg, George R. Welch, Mikhail D. Lukin, Yuri Rostovtsev, Edward S. Fry, and Marlan O. Scully, Phys. Rev. Lett. **82**, 5229 (1999).

[14] A. Dogariu, A. Kuzmich, H. Cao, and L. J. Wang, Opt. Express **8**, 344 (2001).

[15] A. M. Akulshin, A. Cimmino, A. I. Sidorov, P. Hannaford, and G. I. Opat, Phys. Rev. A **67**, 011801(R) (2003).

[16] Eugeniy E. Mikhailov, Vladimir A. Sautenkov, Irina Novikova, and George R. Welch, Phys. Rev. A **69**, 063808 (2004).

[17] Mark Bashkansky, Guy Beadie, Zachary Dutton, Fredrik K. Fatemi, John Reintjes, and Michael Steiner, Phys. Rev. A **72**, 033819 (2005).

[18] Ryan M. Camacho, Michael V. Pack, and John C. Howell, Phys. Rev. A **74**, 033801 (2006).

[19] Ali Javan, Olga Kocharovskaya, Hwang Lee, and Marlan O. Scully, Phys. Rev. A **66**, 013805 (2002).

[20] C. Y. Ye and A. S. Zibrov, Phys. Rev. A **65**, 023806 (2002).

[21] A. Lipsich, S. Barreiro, A. M. Akulshin, and A. Lezama, Phys. Rev. A **61**, 053803 (2000).

[22] L. SpaniMolella, R. H. Rinkleff, and K. Danzmann, Phys. Rev.

[23] F. Renzoni, C. Zimmermann, P. Verkerk, and E. Arimondo, J. Opt. B: Quantum Semiclassical Opt. **3**, S7 (2001).

[24] W. R. Bennett, Phys. Rev. **126**, 580 (1962).

[25] A. Szoke and A. Javan, Phys. Rev. Lett. **10**, 521 (1963).

[26] D. V. Brazhnikov, A. M. Tumaikin, V. I. Yudin, and A. V. Taichenachev, J. Opt. Soc. Am. B **22**, 57 (2005).

[27] D. V. Brazhnikov, A. V. Taichenachev, A. M. Tumaikin, V. I. Yudin, S. A. Zibrov, Ya. O. Dudin, V. V. Vasil'ev, and V. L. Velichansky, JETP Lett. **83**, 64 (2006).

[28] M. M. Mijailović, J. Dimitrijević, A. J. Krmpot, Z. D. Grujić, B. M. Panić, D. Arsenović, D. V. Pantelić, and B. M. Jelenković, Opt. Express **15**, 1328 (2007).

[29] M. L. Harris, C. S. Adams, S. L. Cornish, I. C. McLeod, E. Tarleton, and I. G. Hughes, Phys. Rev. A **73**, 062509 (2006).

[30] Janis Alnis and Marcis Auzinsh, J. Phys. B **34**, 3889 (2001).

[31] Ferruccio Renzoni and Ennio Arimondo, Phys. Rev. A **58**, 4717 (1998).

[32] L. P. Maguire, R. M. W. van Bijnen, E. Mese, and R. E. Scholten, J. Phys. B **39**, 2709 (2006).